Giant dipole resonance and shape transitions in hot and rotating ^{88}Mo

A. K. Rhine Kumar,[1,*] P. Arumugam,[2] N. Dinh Dang,[3,4] and I. Mazumdar[1]

[1]*Department of Nuclear and Atomic Physics, Tata Institute of Fundamental Research, Mumbai - 400 005, India*

[2]*Department of Physics, Indian Institute of Technology Roorkee, Uttarakhand - 247 667, India*

[3]*Quantum Hadron Physics Laboratory, Nishina Center for Accelerator-Based Science, RIKEN 2-1 Hirosawa, Wako City, 351-0198 Saitama, Japan*

[4]*Institute for Nuclear Science and Technique, Hanoi-122100, Vietnam*

(Received 16 November 2016; revised manuscript received 9 June 2017; published 25 August 2017)

The giant dipole resonance (GDR) observables are calculated within the thermal shape fluctuation model by considering the probability distributions of different angular momentum (I) and temperature (T) values estimated recently in the deexcitation process of the compound nucleus ^{88}Mo. These results are found to be very similar to the results obtained with the average T ($T_{\rm ave}$) and average I ($I_{\rm ave}$) corresponding to those distributions. The shape transitions in ^{88}Mo at different T and I are also studied through the free energy surfaces calculated within the microscopic-macroscopic approach. The deformation of ^{88}Mo is found to increase considerably with T and I, leading to the Jacobi shape transition at $I \sim 50\,\hbar$. The combined effect of increasing deformation, larger fluctuations at higher T, and larger Coriolis splitting of GDR components at higher I, leads to a rapid increase in the GDR width.

DOI: 10.1103/PhysRevC.96.024322

I. INTRODUCTION

The exploration of extremes of nuclear landscape has unraveled several interesting phenomena, leading to a better understanding of the nuclear force. The extremes in terms of isospin, density, and spin have received more attention in the recent past, when compared to hot and rotating nuclei. The recent advances in experimental [1–6] and theoretical [7–11] efforts have rekindled the study of hot and rotating nuclei. The giant dipole resonance (GDR) has been considered as a unique and powerful tool to investigate the nuclear structure properties at these extreme conditions. Being a fundamental mode of collective excitation, the GDR can probe nuclei at any excitation and even those with exotic structures [12,13]. The recent GDR studies at extreme isospins also have potential astrophysical implications [14–17]. Hence, it would be interesting to carry out investigations in the cases where there is a clear correlation between the GDR cross sections (or GDR width) and the equilibrium shape of the nucleus. The most important experimental observable for the GDR is the cross section (σ) as a function of the photon energy, from which one can extract the centroid energies and the GDR width (Γ). These observables could effectively reflect the structure of the nuclear state on which the GDR is built.

The properties of the GDR can be explained through macroscopic, microscopic, or a combination of microscopic and macroscopic approaches. The thermal shape fluctuation model (TSFM) is a macroscopic approach [18–21], based on an adiabatic assumption, where the quadrupole shape fluctuations are slow compared with the giant dipole oscillations, so that the latter can feel the changes in the nuclear shape. The TSFM is commonly very successful in explaining the GDR properties at medium temperature (T)($\sim$2 MeV) and high angular momentum (I). Many microscopic models have been developed to explain the GDR, for example, the random-phase approximation method (RPA) [13,22–24], phonon damping model (PDM) [25,26], and the static path approximation (SPA) method [27–29]. The empirical models reported in Refs. [30,31] are also successful in explaining the GDR width at finite T and I.

Several earlier works [32–34] on GDR focused on the high I regime. Beyond a sufficiently large angular momentum (close to the one which the nucleus can sustain without undergoing fission), there could be a transition from the oblate (noncollective) to nearly prolate (collective) shape. Such shape transitions are predicted in gravitating rotating stars [35] and called the Jacobi transition. The exotic shape transitions like the Jacobi transition can also be detected through GDR studies [2,4,10,36,37]. In Ref. [38], the authors mentioned the occurrence of a low-energy GDR component in the GDR spectra as well as the possibility of Jacobi shape transition in ^{88}Mo. The recent experimental efforts have been focusing on more exclusive GDR measurements with a narrow window for tagging the angular momentum. In such a recent work [1], the GDR γ rays emitted from the highly excited ^{88}Mo nucleus that is formed in the reaction ^{48}Ti + ^{40}Ca were measured. The experiment was performed at different excitation energies and compared with the theoretical results obtained from the PDM and Lublin-Strasbourg drop (LSD) model. The data analysis indicates the possibility of Γ saturation at higher I values [1,8]. In this article, we study the GDR properties of the hot and rotating compound nucleus ^{88}Mo at different excitation energies within the TSFM built on the microscopic-macroscopic approach for the free-energy calculations and a macroscopic approach for the GDR calculations [3,6,7,21,39,40]. A short description of our theoretical formalism is presented in the next section followed by the results and the discussion.

*Present address: Department of Physics, Cochin University of Science and Technology, Cochin - 682 022, India; rhinekumar@gmail.com

II. THEORETICAL FRAMEWORK

It is well known that statistical quantities will have more fluctuations if the system is finite [41]. In tiny, finite systems like nuclei, the observables are highly dependent on the fluctuations around the most probable value obtained within the mean-field approach. The simplest solution to this problem is to regard the probability distribution as the Boltzmann factor and to calculate the expectation value of an observable as an average over all possible degrees of freedom. In the study of the structural transitions in hot and rotating nuclei, the most relevant degrees of freedom are the parameters describing the shape of the nucleus (β,γ). The expectation value of an observable $\mathcal{O}$ incorporating thermal shape fluctuations is given by [20,42]

$$\langle\mathcal{O}\rangle_{\beta,\gamma} = \frac{\int_\beta\int_\gamma \mathcal{D}[\alpha]\exp\left[-F_{\rm TOT}(T,I;\beta,\gamma)/T\right]\Im_{\rm TOT}^{-3/2}\mathcal{O}}{\int_\beta\int_\gamma \mathcal{D}[\alpha]\exp\left[-F_{\rm TOT}(T,I;\beta,\gamma)/T\right]\Im_{\rm TOT}^{-3/2}}. \quad (1)$$

The volume element is chosen to be $\mathcal{D}[\alpha] = \beta^4|\sin 3\gamma|\,d\beta\,d\gamma$ and $\Im_{\rm TOT}$ is the moment of inertia. The total free energy ($F_{\rm TOT}$) at a fixed deformation is calculated using the microscopic-macroscopic (Nilsson-Strutinsky) method extended to high spin and temperature [21,40].

The nuclear shapes and the GDR observables are correlated using a macroscopic model which consists of an anisotropic harmonic oscillator potential with a separable dipole-dipole interaction [21,43,44]. The Hamiltonian describing GDR excitations can be written as

$$H = H_{\rm osc} + \eta\, D^\dagger D\,. \quad (2)$$

Here $H_{\rm osc}$ stands for the anisotropic harmonic oscillator Hamiltonian, and η and D represent the dipole-dipole interaction strength and dipole operator, respectively. The total GDR cross section σ is constructed by summing the individual Lorentzians with the peaks at the GDR energies ($E_{\rm i}$) given by the frequencies corresponding to the Hamiltonian (H).

The width of these individual components depend on $E_{\rm i}$ through the relation [45]

$$\Gamma_{\rm i} = \Gamma_0(E_{\rm i}/E_{\rm GDR})^\delta\,, \quad (3)$$

where Γ_0 represents the GDR width at the ground state. Since the width Γ_0 at the ground state is unknown for all the nuclei considered in this work, we chose the value 3.5 MeV which fits the experimental data very well along with the values $\eta = 2$ and $\delta = 1.9$. The GDR energy ($E_{\rm GDR}$) is given by [1,12]

$$E_{\rm GDR} = 18A^{-1/3} + 25A^{-1/6}. \quad (4)$$

In some of the earlier calculations [7,21,40], the energy dependence of the GDR width was dealt purely in an empirical way through the relation [45]

$$\Gamma_{\rm i} = 0.026E_{\rm i}^\delta\,. \quad (5)$$

In such cases the only adjustable parameter of the model is η which can be unambiguously fixed by reproducing the ground-state width if available. However, the relation (5) and subsequently fitted η for the mass region considered are based on older data [21] whereas the recent measurements [1] with more precision are quite different from the older data.

TABLE I. Different daughter nuclei detected along the deexcitation process of compound nucleus ^{88}Mo formed in the reaction ^{48}Ti + ^{40}Ca along with their average T ($T_{\rm ave}$), average I ($I_{\rm ave}$) and the corresponding weight factors (W_ν).

Nucleus (ν)	$T_{\rm ave}$ (MeV)	$I_{\rm ave}$ ($\hbar$)	W_ν
^{88}Mo	3.1	15.17	0.04
^{84}Zr	2.4	28.29	0.51
^{80}Sr	1.6	24.85	0.40
^{76}Kr	0.7	19.56	0.05
^{86}Zr	4.3	29.12	0.19
^{80}Sr	3.6	26.03	0.35
^{74}Se	2.6	18.75	0.30
^{70}Ge	1.6	15.02	0.14
^{68}Ge	0.8	14.46	0.02

III. RESULTS AND DISCUSSION

In nuclear fusion-evaporation reactions, the compound nucleus formed at high T and I deexcites by emitting GDR γ rays, neutrons, and charged particles. This process produces a number of daughter nuclei along the decay path of the compound nucleus with different T and I. The average T ($T_{\rm ave}$) and average I ($I_{\rm ave}$) of the daughter nuclei formed along the decay process will be smaller than the initial T and I of the compound nucleus. In the reaction ^{48}Ti + ^{40}Ca, a number of daughter nuclei created along the cooling path of the compound nucleus ^{88}Mo at different excitation energies were identified experimentally [1]. In this exclusive measurement [1], the GDR γ rays, the recoiling residual nuclei, and the light charged particles were detected. Also, the GDR γ rays emitted from the compound nucleus as well as the different daughter nuclei created in the deexcitation process were measured properly. The statistical model analysis yields the population matrices of different nuclei as a function of T and I [1] from which one can extract the corresponding probability distributions. In Table I, we present the list of different daughter nuclei detected during the deexcitation of compound nucleus ^{88}Mo formed in the reaction ^{48}Ti + ^{40}Ca at two different beam energies. The $T_{\rm ave}$, $I_{\rm ave}$ values obtained from the probability distribution of T and I and the weight factor of different daughter nuclei are also presented [46]. We calculate the average GDR cross section of a nucleus with a given Z and N at a given $T_{\rm ave}$ and having a probability distribution for I as

$$\sigma_{\rm ave}(T_{\rm ave}) = \frac{\sum_i \sigma(T_{\rm ave},I_i)C(i)}{\sum_i C(i)}\,, \quad (6)$$

where I_i are the spins and $C(i)$ are the corresponding spin counts [46].

As the first step, it is very important to analyze whether the average GDR cross sections $\sigma_{\rm ave}(T_{\rm ave})$ of a nucleus obtained by considering the $T_{\rm ave}$ and the probability distribution of I are same as the GDR cross sections $\sigma(T_{\rm ave},I_{\rm ave})$ of a nucleus obtained with the $T_{\rm ave}$ and $I_{\rm ave}$ values obtained from the same

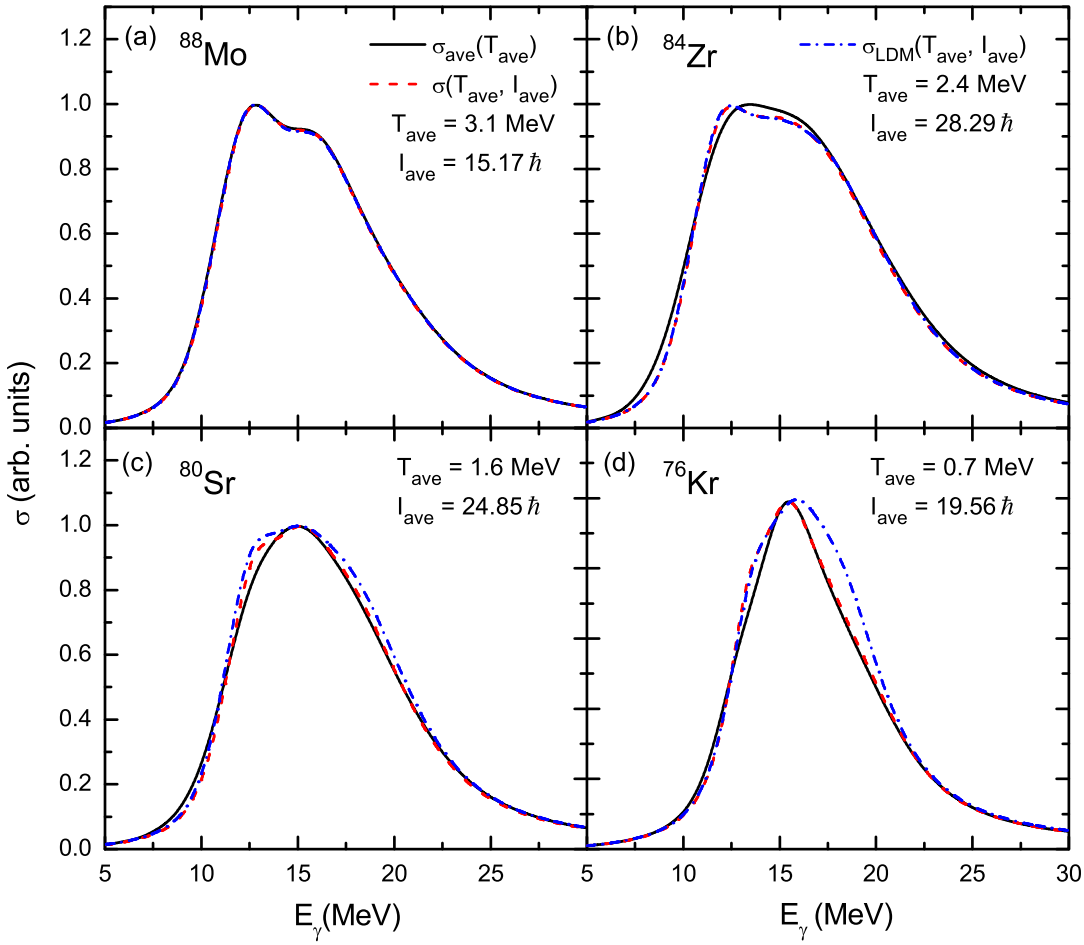

FIG. 1. GDR cross sections (σ) calculated within the TSFM for different daughter nuclei formed at different temperatures (T) in the deexcitation process of the compound nucleus ^{88}Mo obtained with beam energy $E_{\rm lab} = 300$ MeV. The solid line represents the $\sigma_{\rm ave}(T_{\rm ave})$ obtained by considering an average $T_{\rm ave}$ and different angular momentum (I) probability distributions [Eq. (6)]. The dashed line and dash-dotted lines represent the $\sigma(T_{\rm ave}, I_{\rm ave})$ obtained with an average $T_{\rm ave}$ and average $I_{\rm ave}$ given by Eq. (7), respectively. For the latter case, the results obtained by using free energies from the liquid drop model (LDM) are presented as the dash-dotted lines.

probability distributions. The average I is estimated as

$$I_{\rm ave} = \frac{\sum_i I_i C(i)}{\sum_i C(i)} \,. \tag{7}$$

In Fig. 1 we compare the theoretical σ of daughter nuclei produced within the decay path of the compound nucleus ^{88}Mo formed at beam energy $E_{\rm lab} = 300$ MeV. The solid line represents $\sigma_{\rm ave}(T_{\rm ave})$, i.e., the average σ obtained by considering the $T_{\rm ave}$ and the I probability distribution with the weight of each I [Eq. (6)]. The dashed line represents $\sigma(T_{\rm ave}, I_{\rm ave})$, i.e., the σ obtained with the $T_{\rm ave}$ and $I_{\rm ave}$. We have also calculated σ using the liquid drop model (LDM) free energies to see the differences in the results due to shell effects. It is clear from Fig. 1 that shell effects lead to minimal changes at very low T only. The σ obtained with different methods are found to be quite similar.

In order to confirm that the σ obtained with different approaches are similar even at higher excitation energy, we performed similar calculations at a higher beam energy, $E_{\rm lab} = 600$ MeV. In Fig. 2 we compare σ of different daughter nuclei formed in the decay path of the compound nucleus ^{88}Mo formed at higher excitation energy. The $\sigma_{\rm ave}(T_{\rm ave})$ and $\sigma(T_{\rm ave}, I_{\rm ave})$ are similar and hence the trend of these results are the same as seen in the lower beam energy cases.

In Fig. 3(a) we compare the experimental data [1] obtained at $E_{\rm lab} = 300$ MeV with theoretical results ($\sigma^{\rm final}$) obtained by averaging the σ of all daughter nuclei (given in Figs. 1 and 2) with their appropriate weight factors (W_ν) given in Table I.

$$\sigma^{\rm final} = \frac{\sum_\nu \sigma_\nu W_\nu}{\sum_\nu W_\nu} \,. \tag{8}$$

As in Figs. 1 and 2 there are three cases of the final σ ($\sigma^{\rm final}$) originating from $\sigma_{\rm ave}(T_{\rm ave})$, $\sigma(T_{\rm ave}, I_{\rm ave})$, and $\sigma_{\rm LDM}(T_{\rm ave}, I_{\rm ave})$. In Fig. 3(b) the experimental data at $E_{\rm lab} = 600$ MeV are compared with the theoretical results. At both excitation energies, the two methods yield similar results. While the overall conformity of the theoretical results are good with the experimental data, one can note some discrepancies in the low-energy part, especially between $10 < E_\gamma < 15$ MeV. This discrepancy stems from the strong contribution of the low-energy GDR components, which are typical in a macroscopic

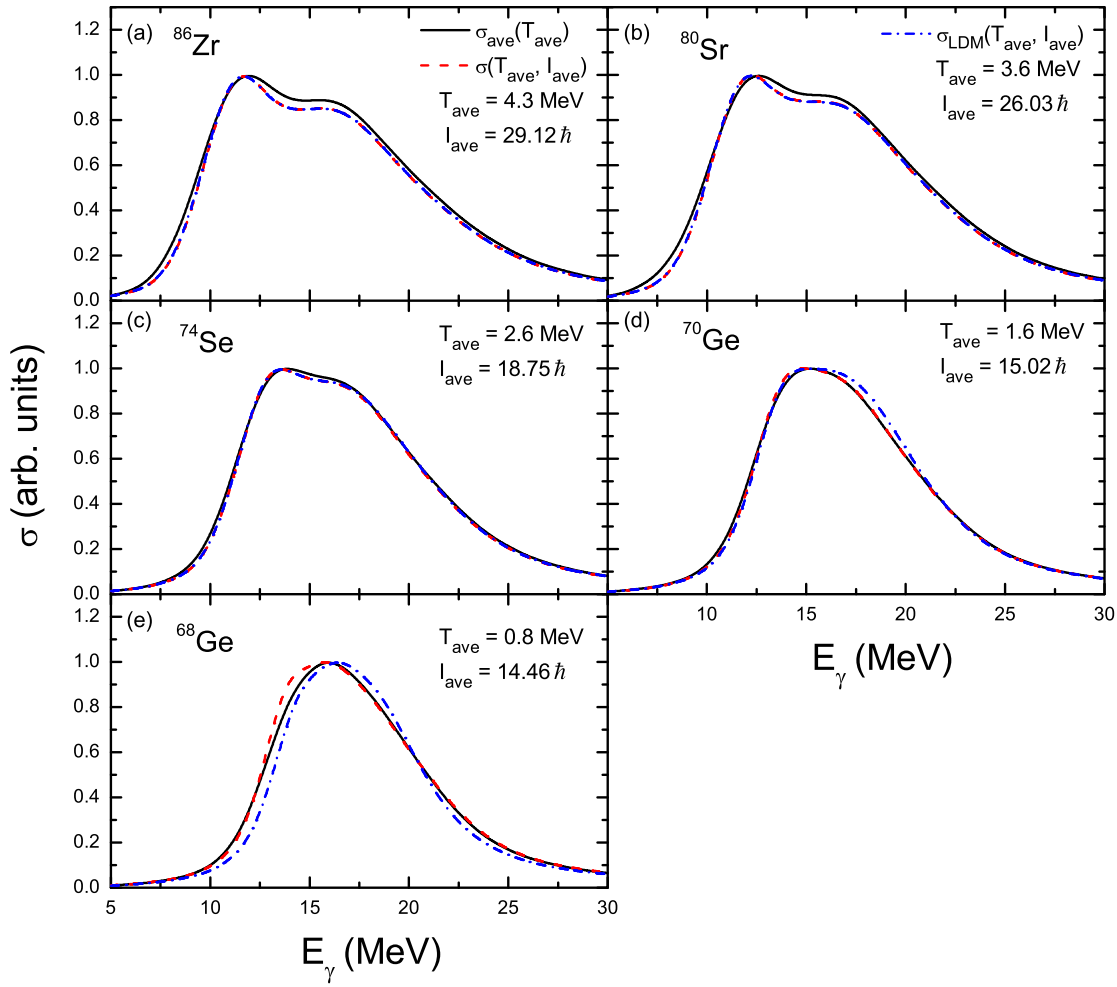

FIG. 2. Same as Fig. 1, but for the beam energy $E_{\rm lab} = 600$ MeV.

approach for GDR with an assumed energy dependence of Γ [Eq. (5)]. This effect gets pronounced at higher excitation where the deformation and Coriolis effects increase the splitting of the GDR components. The GDR strength functions obtained with both PDM and LSD calculations are slightly narrower than the experimental data at the lower energy, whereas the results of our calculations show a better fit with the data. Our results are also in better agreement with the observed high-energy tail at both the energies.

An important conclusion from these results is that it is not necessary to calculate the theoretical σ at each value of T and I obtained in the probability distribution with their respective weights, instead the σ obtained at the average values of T and I are good enough to compare with the experimental data. Normally the $T_{\rm ave}$ and $I_{\rm ave}$ values are smaller than the initial T and I of the compound nucleus.

In Fig. 4, we have compared the GDR width of ^{88}Mo obtained with TSFM with the experimental data. The filled upward triangles connected with solid line, filled downward triangles connected with dashed line, and filled circles connected with dash-dotted line represents the Γ originating from $\sigma^{\rm final}_{\rm ave}(T_{\rm ave})$, $\sigma^{\rm final}(T_{\rm ave}, I_{\rm ave})$, and $\sigma^{\rm final}_{\rm LDM}(T_{\rm ave}, I_{\rm ave})$, respectively, as presented in Fig. 3. All three results are able to explain the experimental Γ at $T = 2$ MeV very well. The Γ originating from $\sigma_{\rm ave}(T_{\rm ave})$ overestimates the experimental data at $T = 3.1$ MeV. We have also presented the Γ (open circles connected with dotted line) obtained with the phonon damping model (PDM) and results obtained with LSD model (upward and downward open triangles connected with lines) taken from Ref. [1] for comparison. The TSFM results yield larger widths than the PDM and this fact can be ascribed to the role of shape fluctuations inherent in TSFM leading to a larger average deformation and hence a larger width. Consequently, the Γ from TSFM does not saturate with T. With the increase in I and the resulting Coriolis splitting of GDR components [43], Γ increases further unless modified by strong transitions in the shape. In our calculations, we assumed that the Γ_0 value is independent of T. In Ref. [1], the authors considered the T dependence of Γ_0 in LSD calculations in order to explain the experimental results. But even after considering the T dependence in Γ_0, the results obtained within the LSD still are not able to describe the GDR width at $T = 2$ MeV, whereas, without considering the T dependence of Γ_0, the LSD model underestimates the GDR width at both temperatures. Our results obtained without considering the T dependence on Γ_0 give a better agreement with the data.

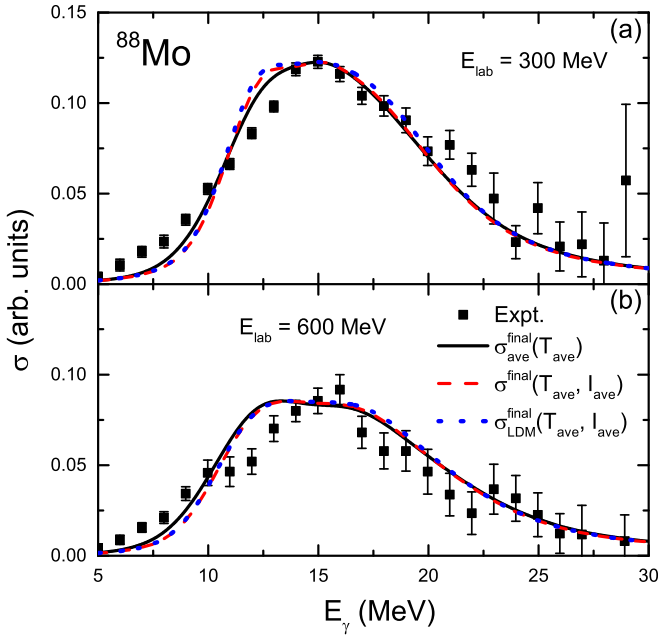

FIG. 3. Experimental GDR cross sections (solid squares) of ^{88}Mo at two different excitation energies taken from Ref. [1], compared with the TSFM results. The solid line represents the average of the GDR cross sections (σ) of daughter nuclei obtained by considering $T_{\rm ave}$ and I probability distributions [Eq. (6)]. The dashed line represents the same obtained with the $T_{\rm ave}$ and $I_{\rm ave}$ with TSFM. For the latter case, the dotted lines represent the calculations with LDM free energies.

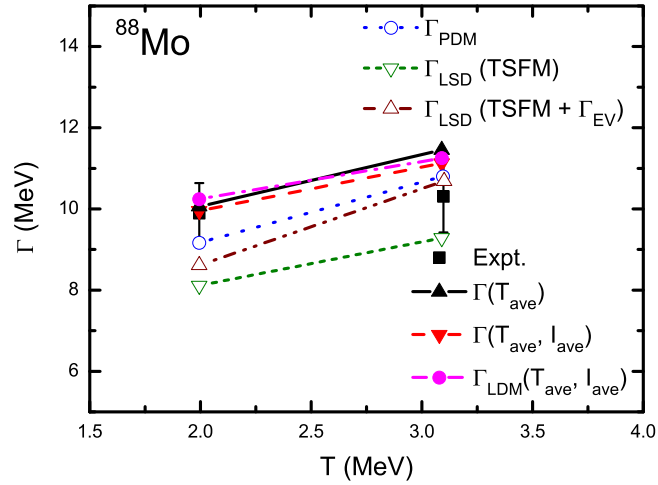

FIG. 4. GDR width Γ of ^{88}Mo calculated using TSFM at two different excitation energies as a function of T. The filled upward triangles connected with solid line represent Γ of the final σ presented in Fig. 3, where σ of the daughter nuclei are obtained by considering the $T_{\rm ave}$ and I probability distributions [Eq. (6)]. The filled downward triangles connected with dashed line and filled circles connected with dash-dotted line represent the Γ of the final σ, where σ of the daughter nuclei are obtained by considering the $T_{\rm ave}$ and $I_{\rm ave}$ within the TSFM with free energies obtained from the microscopic-macroscopic approach and LDM, respectively. The experimental results are taken from Ref. [1]. The widths obtained within the PDM and LSD taken from Ref. [1] are also shown with open circles and open triangles. The lines are drawn just to guide the eyes.

To understand the shape transitions in ^{88}Mo as a function of T and I, we calculated the free-energy surfaces (FES) within the microscopic-macroscopic approach at a few chosen combinations of T and I. The FES obtained at $T = 2$ MeV and $I = 30$, 40, 50, and 60 $\hbar$ are presented in Fig. 5, where we see that the most probable shape of the nucleus is an oblate shape at $I = 30\ \hbar$ and remains so even at high I. As I increases from 30 to 60 $\hbar$, the axial deformation parameter (β) of the nucleus gradually increases from ~0.1 to 0.3. Apart from this smooth change in β, we do not observe any significant shape transition. The features of the FES at lower I remain unaltered at higher T but at $I \sim 60\ \hbar$ our calculations suggest significant shape changes. The FES calculated at $T = 2.5$ and 3 MeV for the cases $I = 55$ and 60 $\hbar$ are presented in Fig. 6. At $T = 2.5$ MeV, the nucleus has an oblate minimum up to $I = 55\ \hbar$, but at $I = 60\ \hbar$, there is a clear and sharp transition to a triaxial shape with the most probable shape having $\beta \sim 0.5$ and $\gamma \sim -150^\circ$. A second minimum at $\beta \sim 0.4$ and $\gamma \sim -180^\circ$ which is an oblate shape has a very low free energy suggesting a coexisting shape. This transition along with the broadening or splitting of the minimum in the FES leads to enhanced fluctuations of the shape. At $T = 3$ MeV, the FES shows gamma-softness with the most probable shape at $\beta = 0.3$ and $\gamma = -180^\circ$ at $I = 55\ \hbar$. At $I = 60\ \hbar$ the minimum moves to $\beta \sim 0.5$ and $\gamma \sim -140^\circ$ which is a nearly prolate shape. This shape transition from a noncollective oblate shape to a collective rotating lightly deformed prolate shape is the Jacobi transition.

To check whether such shape transitions occur at high T, we calculated the FES at $T = 3.5$ MeV and the results are presented in Fig. 7. The nucleus has an oblate shape up to $I = 50\ \hbar$, similar to the results at lower T but with a larger deformation and a shallower minimum. As I increases from 30 to 50 $\hbar$, β increases from 0.1 to 0.3. At $I = 55\ \hbar$ the FES shows a strong gamma-softness with its most probable shape at $\beta \sim 0.45$ and $\gamma = -140^\circ$. The nucleus undergoes the Jacobi transition at $I \sim 55\ \hbar$. At $I = 60\ \hbar$ the FES indicates shape coexistence with its most probable shape at $\beta \sim 0.5$ and $\gamma = -140^\circ$ and a second minimum at $\beta \sim 0.4$ and $\gamma \sim -180^\circ$. In general, the FES calculations show that the nuclear deformation increases with T and I. At higher T, as I increases, the FES shows a gamma-softness before the nucleus undergoes a Jacobi shape transition. All these factors will increase the GDR width at higher T and I and hence the GDR width will not saturate at high T and I. Considering the role of enhanced fluctuations at higher T and the Coriolis splitting of GDR components at higher I, the rate of increase in the GDR width of the ^{88}Mo nucleus increases with the increase in T and I. It is worth mentioning that, in Ref. [10], the authors introduced a new method by combining the LSD model with the collective model; by solving the collective-model Schrödinger equations, one can take into account the large-amplitude nuclear shape fluctuations in the nuclear Jacobi and Poincaré shape transitions.

IV. SUMMARY

The GDR built in the excited states of ^{88}Mo nuclei is studied within the TSFM and compared with recent measurements.

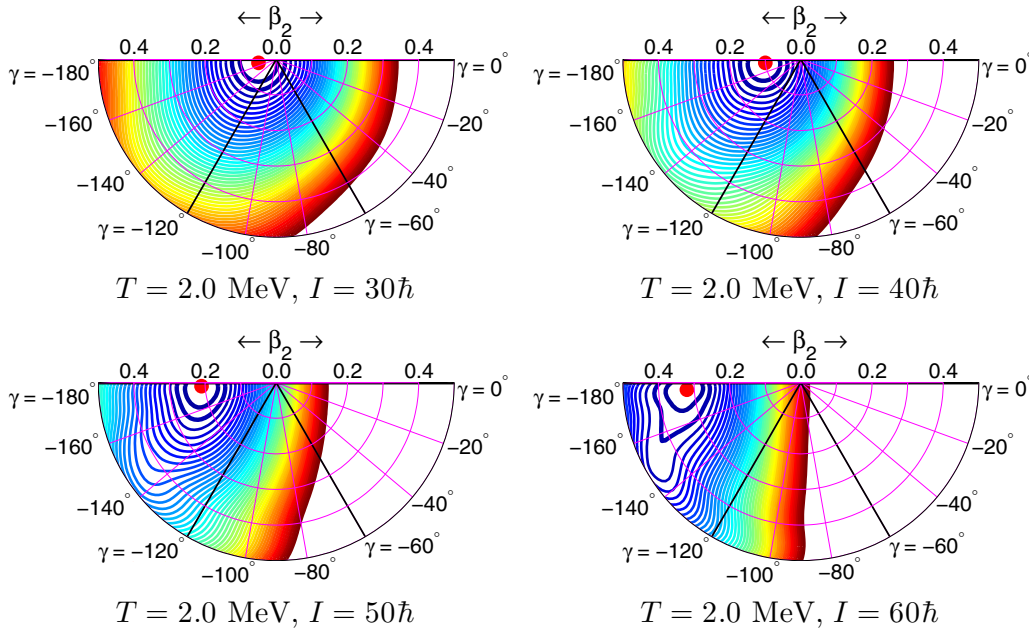

FIG. 5. FES of ^{88}Mo at $T = 2$ MeV with different I. In this convention, $\gamma = 0^\circ$ and -120° represent the noncollective and collective prolate shapes, respectively; $\gamma = -180^\circ$ and -60° represent the noncollective and collective oblate shapes, respectively. The contour line spacing is 0.2 MeV. The most probable shape is represented by a filled circle and first two minima are represented by thicker lines.

The overall agreement with the data is good except for the pronounced low-energy component inherent in the macroscopic description of GDR. It is found that the GDR cross sections of the daughter nuclei formed during the deexcitation process of a compound nucleus according to the probability distributions in temperature (T) and angular momentum (I), are very similar to the GDR cross sections of daughter nuclei obtained with average T ($T_{\rm ave}$) and average I ($I_{\rm ave}$) value. In the range of $2 \lesssim T \lesssim 3$ MeV, the data suggest a slower increase in the GDR width (Γ) whereas the TSFM and the PDM suggest a larger increase. FES calculations for ^{88}Mo reveals that the axial deformation (β) and the shallowness of the minimum increases with I and T. Considering the additional effects of enhanced fluctuations at larger T and larger Coriolis splitting of GDR components, one expects a rapid increase in Γ at higher I and T. The FES calculations depict a clear Jacobi shape transition at $I \sim 55\ \hbar$ leading to highly deformed shapes which is more favored at higher T.

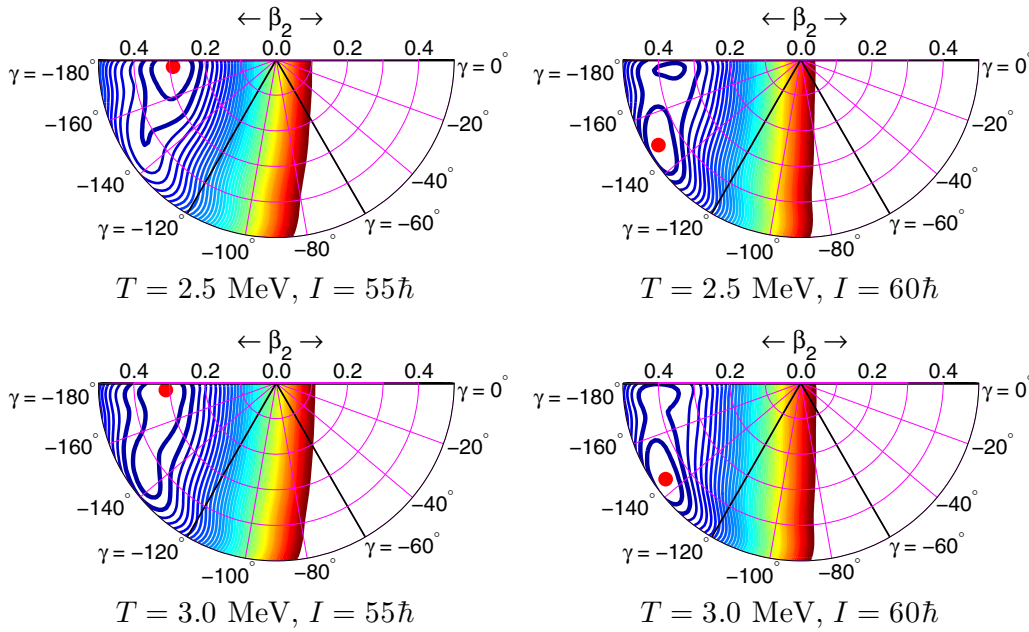

FIG. 6. Same as Fig. 5, but at $T = 2.5$ and 3 MeV.

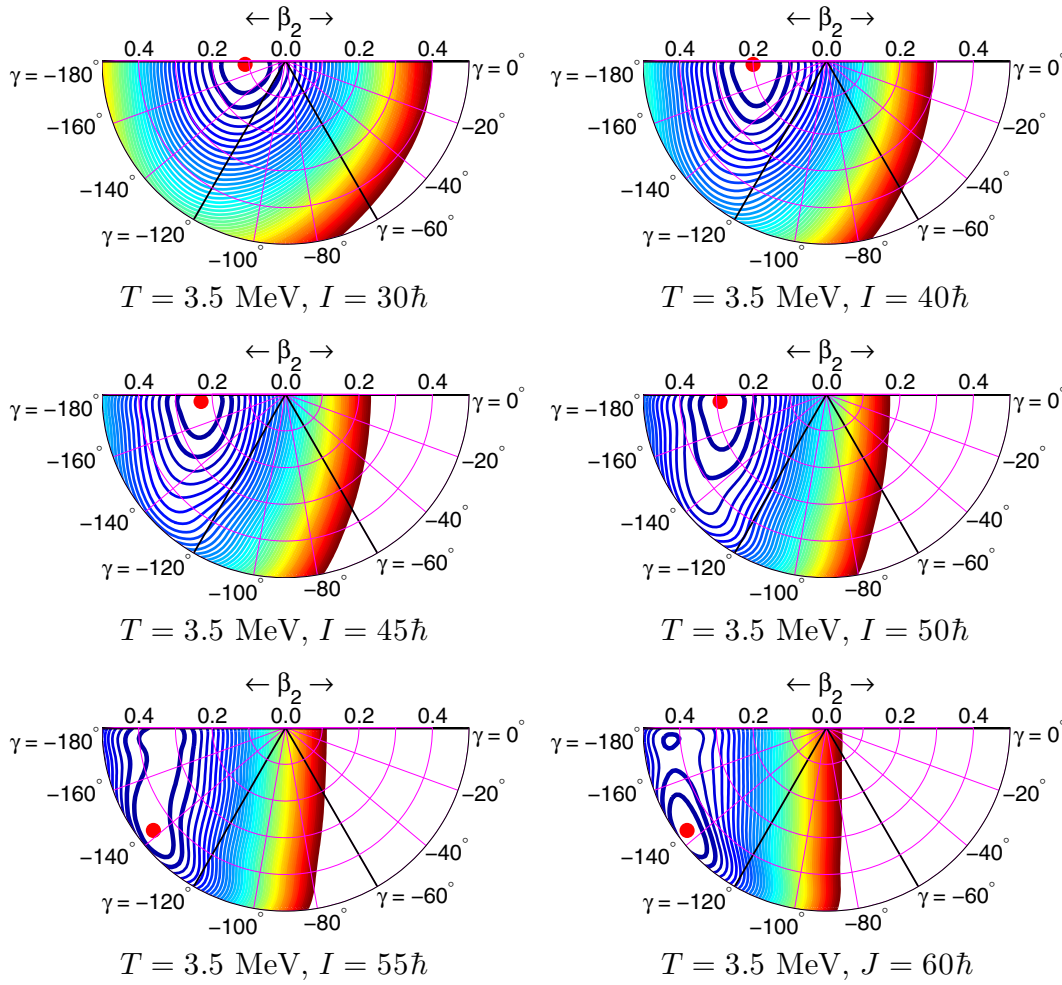

FIG. 7. Same as Fig. 5, but at $T = 3.5$ MeV.

ACKNOWLEDGMENTS

The authors thank M. Ciemala, M. Kmiecik, and A. Maj for providing the experimental data and for their fruitful discussions and suggestions. We acknowledge financial support from the Science and Engineering Research Board (India), DST/INT/POL/P-09/2014. The numerical calculations were carried out using RIKEN Supercomputer HOKUSAI GreatWave System. A.K.R.K. would like to thank DST-INSPIRE Faculty programe, Government of India.

[1] M. Ciemała, M. Kmiecik, A. Maj, K. Mazurek, A. Bracco, V. L. Kravchuk, G. Casini, S. Barlini, G. Baiocco, L. Bardelli *et al.*, Phys. Rev. C **91**, 054313 (2015).

[2] D. R. Chakrabarty, V. M. Datar, S. Kumar, G. Mishra, E. T. Mirgule, A. Mitra, P. C. Rout, V. Nanal, D. Pandit, S. Mukhopadhyay *et al.*, Phys. Rev. C **85**, 044619 (2012).

[3] C. Ghosh, G. Mishra, A. K. R. Kumar, N. Dokania, V. Nanal, R. G. Pillay, S. Kumar, P. C. Rout, S. Joshi, and P. Arumugam, Phys. Rev. C **94**, 014318 (2016).

[4] D. Pandit, S. Mukhopadhyay, S. Bhattacharya, S. Pal, A. De, S. Bhattacharya, C. Bhattacharya, K. Banerjee, S. Kundu, T. K. Rana *et al.*, Phys. Rev. C **81**, 061302 (2010).

[5] D. Pandit, B. Dey, D. Mondal, S. Mukhopadhyay, S. Pal, S. Bhattacharya, A. De, and S. R. Banerjee, Phys. Rev. C **87**, 044325 (2013).

[6] I. Mukul, A. Roy, P. Sugathan, J. Gehlot, G. Mohanto, N. Madhavan, S. Nath, R. Dubey, I. Mazumdar, D. A. Gothe *et al.*, Phys. Rev. C **88**, 024312 (2013).

[7] A. K. Rhine Kumar and P. Arumugam, Phys. Rev. C **92**, 044314 (2015).

[8] N. D. Dang, M. Ciemala, M. Kmiecik, and A. Maj, Phys. Rev. C **87**, 054313 (2013).

[9] N. D. Dang, Phys. Rev. C **85**, 064323 (2012).

[10] K. Mazurek, J. Dudek, A. Maj, and D. Rouvel, Phys. Rev. C **91**, 034301 (2015).

[11] T. Sil, S. Shlomo, B. K. Agrawal, and P.-G. Reinhard, Phys. Rev. C **73**, 034316 (2006).

[12] J. J. Gaardhøje, Annu. Rev. Nucl. Part. Sci. **42**, 483 (1992).

[13] K. A. Snover, Annu. Rev. Nucl. Part. Sci. **36**, 545 (1986).

[14] D. M. Rossi, P. Adrich, F. Aksouh, H. Alvarez-Pol, T. Aumann, J. Benlliure, M. Böhmer, K. Boretzky, E. Casarejos, M. Chartier *et al.*, Phys. Rev. Lett. **111**, 242503 (2013).

[15] J. Endres, E. Litvinova, D. Savran, P. A. Butler, M. N. Harakeh, S. Harissopulos, R.-D. Herzberg, Krücken, A. Lagoyannis, N. Pietralla *et al.*, Phys. Rev. Lett. **105**, 212503 (2010).

[16] T. Li, U. Garg, Y. Liu, R. Marks, B. K. Nayak, P. V. M. Rao, M. Fujiwara, H. Hashimoto, K. Nakanishi, S. Okumura *et al.*, Phys. Rev. C **81**, 034309 (2010).
[17] A. Makinaga, R. Massarczyk, R. Schwengner, M. Beard, F. Donau, M. Anders, D. Bemmerer, R. Beyer, R. Hannaske, A. R. Junghans *et al.*, Phys. Rev. C **90**, 044301 (2014).
[18] Y. Alhassid, B. Bush, and S. Levit, Phys. Rev. Lett. **61**, 1926 (1988).
[19] Y. Alhassid and B. Bush, Nucl. Phys. A **509**, 461 (1990).
[20] Y. Alhassid, Nucl. Phys. A **649**, 107c (1999).
[21] P. Arumugam, G. Shanmugam, and S. K. Patra, Phys. Rev. C **69**, 054313 (2004).
[22] J. Meyer, P. Quentin, and M. Brack, Phys. Lett. B **133**, 279 (1983).
[23] H. Sagawa and G. Bertsch, Phys. Lett. B **146**, 138 (1984).
[24] K. Goeke and J. Speth, Annu. Rev. Nucl. Part. Sci. **32**, 65 (1982).
[25] N. D. Dang, K. Tanabe, and A. Arima, Phys. Lett. B **445**, 1 (1998).
[26] N. D. Dang and A. Arima, Nucl. Phys. A **636**, 427 (1998).
[27] A. Ansari, N. D. Dang, and A. Arima, Phys. Rev. C **62**, 011302(R) (2000).
[28] Y. Alhassid and J. Zingman, Phys. Rev. C **30**, 684 (1984).
[29] B. Lauritzen and G. Bertsch, Phys. Rev. C **39**, 2412 (1989).
[30] D. Kusnezov, Y. Alhassid, and K. A. Snover, Phys. Rev. Lett. **81**, 542 (1998).
[31] D. Pandit, S. Mukhopadhyay, S. Pal, A. De, and S. R. Banerjee, Phys. Lett. B **713**, 434 (2012).
[32] M. Kmiecik, A. Maj, A. Bracco, F. Camera, M. Casanova, S. Leoni, B. Million, B. Herskind, R. Bark, and W. E. Ormand, Nucl. Phys. A **674**, 29 (2000).
[33] D. R. Chakrabarty, V. Nanal, V. M. Datar, S. Kumar, A. Mitra, E. T. Mirgule, and R. G. Pillay, Nucl. Phys. A **770**, 126 (2006).
[34] F. Camera, A. Bracco, S. Leoni, B. Million, M. Mattiuzzi, M. Pignanelli, A. Maj, M. Kmiecik, R. Bark, J. Bearden *et al.*, Phys. Rev. C **60**, 014306 (1999).
[35] S. Chandrasekhar, Commun. Pure Appl. Math. **20**, 251 (1967).
[36] A. Maj, M. Kmiecik, A. Bracco, F. Camera, P. Bednarczyk, B. Herskind, S. Brambilla, G. Benzoni, M. Brekiesz, D. Curien *et al.*, Nucl. Phys. A **731**, 319 (2004).
[37] N. Schunck, J. Dudek, and B. Herskind, Phys. Rev. C **75**, 054304 (2007).
[38] M. Ciemala, M. Kmiecik, V. Kravchuk, A. Maj, S. Barlini, G. Casini, F. Gramegna, F. Camera, A. Corsi, L. Bardelli *et al.*, Acta Phys. Pol. B **42**, 633 (2011).
[39] I. Mukul, A. Roy, P. Sugathan, J. Gehlot, G. Mohanto, S. Nath, N. Madhavan, R. Dubey, T. Banerjee, N. Saneesh *et al.*, J. Phys. G: Nucl. Part. Phys. **41**, 115103 (2014).
[40] P. Arumugam, A. G. Deb, and S. K. Patra, Eur. Phys. J. A **25**, 199 (2005).
[41] L. D. Landau and E. M. Lifshitz, *Statistical Physics: Part 1 (Course of Theoretical Physics)*, Vol. 5 (Pergamon, Oxford, 1980), 3rd ed.
[42] Y. Alhassid and B. Bush, Nucl. Phys. A **531**, 39 (1991).
[43] R. R. Hilton, Z. Phys. A **309**, 233 (1983).
[44] G. Shanmugam and M. Thiagasundaram, Phys. Rev. C **37**, 853 (1988).
[45] P. Carlos, R. Bergere, H. Beil, A. Lepretre, and A. Veyssiere, Nucl. Phys. A **219**, 61 (1974).
[46] M. Ciemała (private communication).